doi:10.1093/brain/awu079 Brain 2014: 137; 1627–1642 | 1627

BRAIN
A JOURNAL OF NEUROLOGY

Gain-of-function mutations in sodium channel $Na_V1.9$ in painful neuropathy

Jianying Huang,[1,*] Chongyang Han,[1,*] Mark Estacion,[1,*] Dymtro Vasylyev,[1,*] Janneke G. J. Hoeijmakers,[2] Monique M. Gerrits,[3] Lynda Tyrrell,[1] Giuseppe Lauria,[4] Catharina G. Faber,[2] Sulayman D. Dib-Hajj,[1] Ingemar S. J. Merkies[2,5] and Stephen G. Waxman[1] on behalf of the PROPANE Study Group

1 Department of Neurology, Yale University School of Medicine, New Haven, CT 06510, and Centre for Neuroscience and Regeneration Research, Veterans Affairs Medical Centre, West Haven, CT 06516, USA
2 Department of Neurology, University Medical Centre Maastricht, Maastricht, The Netherlands
3 Department of Clinical Genetics, University Medical Centre Maastricht, Maastricht, The Netherlands
4 Neuromuscular Diseases Unit and Bioinformatics Unit, IRCCS Foundation, 'Carlo Besta', Neurological Institute Milan, Italy
5 Department of Neurology, Spaarne Hospital, Hoofddorp, The Netherlands

*These authors contributed equally to this work.

Correspondence to: Stephen G. Waxman, M.D. Ph.D.,
Neuroscience and Regeneration Research Centre,
VA Connecticut Healthcare System,
950 Campbell Avenue,
Bldg. 34, West Haven,
CT 06516, USA
E-mail: stephen.waxman@yale.edu

Sodium channel $Na_v1.9$ is expressed in peripheral nociceptive neurons, as well as visceral afferents, and has been shown to act as a threshold channel. Painful peripheral neuropathy represents a significant public health challenge and may involve gain-of-function variants in sodium channels that are preferentially expressed in peripheral sensory neurons. Although gain-of-function variants of peripheral sodium channels $Na_v1.7$ and $Na_v1.8$ have recently been found in painful small fibre neuropathy, the aetiology of peripheral neuropathy in many cases remains unknown. We evaluated 459 patients who were referred for possible painful peripheral neuropathy, and confirmed the diagnosis of small fibre neuropathy in a cohort of 393 patients (369 patients with pure small fibre neuropathy, and small fibre neuropathy together with large fibre involvement in an additional 24 patients). From this cohort of 393 patients with peripheral neuropathy, we sequenced *SCN11A* in 345 patients without mutations in *SCN9A* and *SCN10A*, and found eight variants in 12 patients. Functional profiling by electrophysiological recordings showed that these $Na_v1.9$ mutations confer gain-of-function attributes to the channel, depolarize resting membrane potential of dorsal root ganglion neurons, enhance spontaneous firing, and increase evoked firing of these neurons. Our data show, for the first time, missense mutations of $Na_v1.9$ in individuals with painful peripheral neuropathy. These genetic and functional observations identify missense mutations of $Na_v1.9$ as a cause of painful peripheral neuropathy.

Keywords: sensory neurons; voltage-clamp; current-clamp; DRG; channelopathy

Abbreviations: DRG = dorsal root ganglion; RMP = resting membrane potential; TTX = tetrodotoxin

Received December 27, 2013. Revised February 21, 2014. Accepted February 22, 2014. Advance Access publication April 27, 2014

Introduction

Painful peripheral neuropathy represents an unmet medical challenge (Hoeijmakers *et al.*, 2012*a*). Recently, Faber *et al*. (2012*a*, *b*) reported gain-of-function missense variants in sodium channels $Na_v1.7$ and $Na_v1.8$, which are abundantly expressed in spinal sensory (dorsal root ganglion, DRG) neurons and their axons within peripheral nerves (Black and Waxman, 2002; Persson *et al.*, 2010; Black *et al.*, 2012), in patients with a diagnosis of painful small fibre neuropathy according to the international criteria (Tesfaye *et al.*, 2010; Hoeijmakers *et al.*, 2012*a*). Although the majority of cases with small fibre neuropathy are of unknown aetiology, the involvement of $Na_v1.7$ and $Na_v1.8$ suggests that other sodium channels that are expressed within peripheral sensory neurons may also harbour variants that may be linked to painful neuropathy.

$Na_v1.9$, initially termed NaN (Dib-Hajj *et al.*, 1998) or SNS2 (Tate *et al.*, 1998), is preferentially expressed within peripheral DRG, trigeminal and myenteric neurons (Dib-Hajj *et al.*, 1998, 2002; Rugiero *et al.*, 2003), and has been found within free nerve terminals in skin and cornea (Black and Waxman, 2002; Dib-Hajj *et al.*, 2002; Persson *et al.*, 2010). $Na_v1.9$ current is resistant to tetrodotoxin (TTX), with a distinctive hyperpolarized voltage-dependence of activation close to the resting membrane potential of most neurons (−60 to −70 mV) and broad overlap between activation and steady-state inactivation predicting that it should produce a persistent current (Cummins *et al.*, 1999). Current-clamp recordings and computer simulation studies have shown that $Na_v1.9$ acts as a threshold channel that regulates excitability of DRG neurons (Herzog *et al.*, 2001; Baker *et al.*, 2003; Ostman *et al.*, 2007).

Animal studies have suggested that $Na_v1.9$ plays a role in pain signalling (Dib-Hajj *et al.*, 2010). Recently, a gain-of-function mutation in *SCN11A*, the gene that encodes $Na_v1.9$, was reported to be linked to two rare genetic disorders: congenital insensitivity to pain (Leipold *et al.*, 2013), and familial episodic pain (Zhang *et al.*, 2013). Here we describe missense mutations in $Na_v1.9$ in patients with painful peripheral neuropathy. We show by voltage-clamp, current-clamp and dynamic clamp electrophysiology that these mutations alter gating properties of the channel and increase spontaneous firing and evoked firing of DRG neurons. These genetic and functional observations link gain-of-function $Na_v1.9$ variants to a common neurological disorder, painful peripheral neuropathy.

Materials and methods

All human studies were approved by an institutional review board at Maastricht University Medical Centre. All aspects of the study were explained to all patients, and written informed consent was obtained before study initiation.

SCN11A mutation analysis

Genomic DNA was extracted from blood using the Puregene® genomic DNA isolation kit (Gentra-Systems). All coding exons and flanking intronic sequences were amplified and sequenced as described previously (Faber *et al.*, 2012*a*). Genomic sequences were compared with reference $Na_v1.9$ complementary DNA (NM_014139.2) to identify sequence variations (Dib-Hajj *et al.*, 1999) using Alamut Mutation-Interpretation Software (Interactive-Biosoftware). A control panel of DNA from healthy 224 and 470 chromosomes from The Netherlands and the UK, respectively, were screened for all new mutations. The NCBI SNP database, the Human Gene Mutation Database (HGMD®), the 1000 Genomes project (www.1000genomes.org/data), and the Human EVS database were also screened.

Plasmids

Human $Na_v1.9$ was amplified from human DRG neuron complementary DNA template (Dib-Hajj *et al.*, 1999), and cloned into a modified pcDNA3 vector designed to be a low-copy number plasmid (Klugbauer *et al.*, 1995). Using Mega mutagenesis protocol, a sequence encoding enhanced green fluorescent protein was cloned upstream of the $Na_v1.9$ ATG with a 'stopGo' 33 amino acid 2A linker, such that the GFP-2A adaptor and the $Na_v1.9$ channel proteins are produced as independent proteins from the same messenger RNA (Ryan and Drew, 1994; Atkins *et al.*, 2007; Luke *et al.*, 2008). In pilot experiments, we confirmed the presence of GFP-2A and $Na_v1.9$ channels as independent proteins on western blots, and demonstrated that the channel produces the expected TTX-resistant ultra-slow inactivating current (data not shown). The c.1142T>C (p.Ile381Thr) and c.3473T>C (p.Leu1158Pro) mutations were introduced into the construct using QuikChange® II XL site-directed mutagenesis (Stratagene) and referred to as I381T and L1158P channels hereinafter.

Dorsal root ganglion neuron isolation and transfection for voltage-clamp studies

Animal studies followed a protocol approved by the Veterans Administration Connecticut Healthcare System Institutional Animal Care and Use Committees. For voltage-clamp recording, DRG neurons were isolated, as previously reported (Dib-Hajj *et al.*, 2009), from 4–8 week old $Na_v1.9$ knock-out mice (Ostman *et al.*, 2007) and transfected by electroporation. Briefly, DRGs were harvested, incubated at 37°C for 20 min in complete saline solution (in mM: 137 NaCl, 5.3 KCl, 1 $MgCl_2$, 25 sorbitol, 3 $CaCl_2$, and 10 HEPES, adjusted to pH 7.2 with NaOH) containing 0.5 U/ml Liberase TM (Roche Diagnostics) and 0.6 mM EDTA before 15 min incubation at 37°C in complete saline solution containing 0.5 U/ml Liberase TL (Roche Diagnostics), 0.6 mM EDTA, and 30 U/ml papain (Worthington Biochemical). Tissue was then centrifuged and triturated in 0.5 ml of DRG media: Dulbecco's Modified Eagle Medium/F12 (1:1) with 100 U/ml penicillin, 0.1 mg/ml streptomycin (Invitrogen) and 10% foetal bovine serum (Hyclone), containing 1.5 mg/ml bovine serum albumin (low endotoxin) and 1.5 mg/ml trypsin inhibitor (Sigma). After trituration, the cell suspension was transfected with wild-type or mutant $Na_v1.9$ constructs with a Nucleofector IIS device (Lonza), using the Amaxa® Basic Neuron SCN Nucleofector™ Kit (VSPI-1003) and SCN Basic Neuro Protocol 6. Briefly, the cell suspension was centrifuged (100 *g* for 3 min), the supernatant was carefully removed, and the cell pellet was resuspended in 20 µl Nucleofector™ solution, mixed with 2.5 µg of wild-type human $Na_v1.9$ or mutant construct, and transfected. After electroporation, 100 µl of calcium-free Dulbecco's modified Eagle medium (Invitrogen) was added and cells were incubated at 37°C for 5 min in a 95% air/5% (vol/vol) CO_2 incubator to allow neurons to recover. The cell mixture was then diluted with DRG media containing 1.5 mg/ml bovine serum albumin (low endotoxin)

and 1.5 mg/ml trypsin inhibitor, seeded onto poly-D-lysine/laminin-coated coverslips (BD) and incubated at 37°C to allow DRG neurons to attach to the coverslips. After 40 min, DRG media was added into each well to a final volume of 1.4 ml and the DRG neurons were maintained at 37°C in a 95% air/5% (vol/vol) CO_2 incubator for 40 h before voltage-clamp recording.

Voltage-clamp recordings

Voltage-clamp recordings were obtained at 22 ± 1°C, 40–48 h after transfection using an EPC-10 amplifier (HEKA Electronics). Small DRG neurons (<25 μm) with robust green fluorescence and no apparent neurites were selected for voltage-clamp recording. Pipette potential was adjusted to zero before seal formation, and liquid junction potential was not corrected. Capacity transients were cancelled and voltage errors minimized with ~90% series resistance compensation. Voltage-dependent currents were acquired with Patchmaster at 5 min after establishing whole-cell configuration, sampled at 50 kHz, and filtered at 2.9 kHz. The pipette solution contained (in mM): 140 CsF, 10 NaCl, 1 EGTA, and 10 HEPES, pH 7.3 with CsOH (adjusted to 315 mOsmol/l with dextrose). The extracellular bath solution contained (in mM): 140 NaCl, 3 KCl, 1 $MgCl_2$, 1 $CaCl_2$, 10 HEPES, 5 CsCl, 20 tetraethylammonium chloride (TEA·Cl), pH 7.3 with NaOH (327 mOsmol/l). TTX (500 nM), $CdCl_2$ (0.1 mM), and 4-aminopyridine (1 mM) were added in the bath solution to block endogenous TTX-sensitive (sensitive) voltage-gated sodium currents, calcium currents, and potassium currents, respectively.

Initially, neurons were held at −100 mV, and a series of 100-ms step depolarizations from −100 to −20 mV were applied in 5 mV increments at 5 s intervals to record the total TTX-resistant current. The neurons were then held at −60 mV and depolarized through a series of test pulses following a 100 ms step to −100 mV to inactivate $Na_v1.9$, leaving the $Na_v1.8$ current intact. The $Na_v1.8$ current could then be subtracted from the total TTX-resistant current in order to isolate the $Na_v1.9$ current (Cummins *et al.*, 1999). Activation curves were obtained by converting I to conductance (G) at each voltage (V) using the equation $G = I / (V - V_{rev})$, where V_{rev} is the reversal potential, which was determined for each cell individually. Activation curves were then fit with Boltzmann functions in the form of $G = G_{max} / \{1 + exp[(V_{1/2,act} - V) / k]\}$, where G_{max} is the maximal sodium conductance, $V_{1/2,act}$ is the potential at which activation is half-maximal, V is the test potential and k is the slope factor.

Steady-state fast-inactivation was assessed with a series of 500 ms prepulses (−140 to 0 mV in 10-mV increments) and the remaining non-inactivated channels were activated by a 50-ms step depolarization to −45 mV (a voltage at which $Na_v1.8$ channel does not open). Steady-state slow-inactivation was determined with 30 s prepulses ranging from −120 to −30 mV followed by a 100 ms pulse to −100 mV to remove fast-inactivation; prepulse was from −130 for I381T mutant as the plateau was not reached at −120 mV (Fig. 4E). Remaining available channels were activated by a 50 ms test pulse to −45 mV. Peak inward currents obtained from steady-state fast-inactivation and slow-inactivation protocols were normalized to the maximal peak current (I_{max}) and fit with Boltzmann functions: $I / I_{max} = A + (1 - A) / \{1 + exp[(V - V_{1/2,inact}) / k]\}$, where V represents the inactivating prepulse potential, $V_{1/2,inact}$ represents the midpoint of the steady-state fast-inactivation or slow-inactivation.

Deactivation was estimated from current decay, using a 25 ms short depolarizing pulse to −45 mV followed by a 150 ms repolarizing pulse to potentials ranging from −110 to −70 mV with 5-mV increments. Deactivation kinetics were calculated by fitting the decaying currents with a single exponential function.

Dorsal root ganglion neuron isolation and transfection for current-clamp studies

DRGs from 4- to 8-week-old Sprague Dawley rats were harvested and dissociated as described previously (Dib-Hajj *et al.*, 2009). Briefly, DRG were dissociated with a 20 min incubation at 37°C in complete saline solution containing 1.5 mg/ml Collagenase A (Roche Diagnostics) and 0.6 mM EDTA, followed by a 20-min incubation at 37°C in complete saline solution containing 1.5 mg/ml Collagenase D (Roche Diagnostics), 0.6 mM EDTA, and 30 U/ml papain. A suspension of DRG neurons was then prepared as described above, 2 ml of DRG media was added to the suspension and the suspension filtered using a 70 μm nylon cell strainer (Becton Dickinson). The cell strainer was washed with 2 × 2 ml of DRG media, the washes were combined with the suspension and then centrifuged at 100 *g* for 3 min, the supernatant removed and cells transfected as described above using the Amaxa® Basic Neuron SCN Nucleofector™ Kit (VSPI-1003) and SCN Basic Neuro Protocol 6. After electroporation, cells were treated as described above except that 30–40 min after seeding DRG media was added to each well to a final volume of 1.0 ml containing nerve growth factor (50 ng/ml) and glial cell line-derived neurotrophic factor (50 ng/ml).

Current-clamp recordings

Current-clamp recordings were obtained as previously described (Faber *et al.*, 2012*b*) from small (<30-μm diameter) green fluorescent protein-labelled DRG neurons 40–48 h after transfection using EPC-10 (HEKA) amplifier. Electrodes had a resistance of 1–3 MΩ when filled with the pipette solution, which contained (in mM): 140 KCl, 0.5 EGTA, 5 HEPES, and 3 Mg-ATP, pH 7.3 with KOH (adjusted to 315 mOsm with dextrose). The extracellular solution contained (in mM): 140 NaCl, 3 KCl, 2 $MgCl_2$, 2 $CaCl_2$, 10 HEPES, pH 7.3 with NaOH (adjusted to 320 mOsm with dextrose). Whole-cell configuration was obtained in voltage-clamp mode before proceeding to current-clamp recording mode. Cells with action potential overshoot of <40 mV were excluded for data collection. Threshold was determined by the first action potential elicited by a series of 200-ms depolarizing current injections that increased in 5 pA increments. For comparison with our previous current-clamp studies on neuropathy-associated mutations of $Na_v1.7$ (Faber *et al.*, 2012*a*) and $Na_v1.8$ (Faber *et al.*, 2012*b*), the response to a graded series of 500 ms current stimuli from 25 to 500 pA, in 25 pA increments, was assessed.

Data analysis

Electrophysiological data were analysed using Fitmaster (HEKA Electronics) and Origin 8.5.1 (Microcal), and presented as means ± standard error (SE). Statistical significance was determined by unpaired Student's *t*-tests (current-clamp except firing frequency and spontaneous activity), paired Student's *t*-test [measurement of changes in current threshold corresponding to resting membrane potential (RMP) alterations], Mann-Whitney test (firing frequency) or two-proportion *z*-test (comparison of proportion of cells producing spontaneous activity).

Controls for voltage- and current-clamp

To minimize inherent culture-to-culture variability and to overcome the possibility of error induced by pooling the results of experiments on

DRG neurons harvested from multiple animals and cultured over many months, each mutant was compared by voltage- and current-clamp with contemporaneous controls of wild-type human $Na_v1.9$ expressed in cultures of cells prepared, transfected and recorded under identical conditions by the same physiologist.

Dynamic clamp recording

DRG neurons obtained from adult $Na_v1.9$ knockout mice were enzymatically isolated as described previously (Dib-Hajj *et al.*, 2009; Ahn *et al.*, 2013) and were used for dynamic clamp recording within 12 h *in vitro*. Small DRG neurons (soma diameter $<25\,\mu m$) were dynamically clamped (Sharp *et al.*, 1993; Kemenes *et al.*, 2011; Samu *et al.*, 2012) in whole-cell configuration using patch pipettes pulled from glass capillaries (World Precision Instruments; catalogue number PG10165-4). Pipette resistance was 2–3 MΩ when filled with the intracellular solution (in mM): 140 KCl; 3 MgATP, 0.5 EGTA, 5 HEPES; 10 glucose, pH 7.3 with KOH (adjusted to 325 mOsm with sucrose). The extracellular solution was Hank's Balanced Salt Solution (Invitrogen, catalogue number 14025) (in mM): 1.3 $CaCl_2$, 0.5 $MgCl_2$, 0.4 $MgSO_4$, 5.3 KCl, 0.4 KH_2PO_4, 4.2 $NaHCO_3$, 138 NaCl, 0.3 Na_2HPO_4, 5.6 glucose (adjusted to 325 mOsm with sucrose). Liquid junction potential (+3.8 mV) between pipette and bath solutions was compensated. Membrane voltages and currents were recorded in dynamic-clamp using MultiClamp 700B amplifier (Molecular Devices) interfaced with CED Power 1401 mk II DAI and Signal software (CED), digitized by Digidata 1440A DAC and stored on the hard disk using pCLAMP 10 software (Molecular Devices). Voltage and current traces were filtered at 10 kHz and digitized at 50 kHz. Recordings were made at room temperature (22–23°C). All data are presented as means ± SE. Data were analysed using pCLAMP 10 (Molecular Devices), and Origin 8.5 (OriginLab) software. The hypothesis that population means are significantly different was assessed using Student's *t*-test or Mann-Whitney non-parametric test, when appropriate ($*P < 0.05$; $**P < 0.01$).

Kinetic model of $Na_v1.9$ channel

$Na_v1.9$ channel model used for dynamic clamp was based on Hodgkin-Huxley equations $dm/dt = \alpha_m(1 - m) - \beta_m m$; $dh/dt = \alpha_h(1 - h) - \beta_h h$; $ds/dt = \alpha_s(1 - s) - \beta_s s$, where m, h and s are channel activation, fast- and slow-inactivation variables, and α (β) are forward (backward) rate constants, respectively. The following rate constants were used for the wild-type $Na_v1.9$ channel model:

$$\alpha_m = 0.751/(1 + \exp(-(V + 32.26)/13.71)),$$
$$\beta_m = 5.68/(1 + \exp((V + 123.71)/13.94));$$

$$\alpha_h = 0.082/(1 + \exp((V + 113.69)/17.4)),$$
$$\beta_h = 0.24/(1 + \exp(-(V - 10.1)/17.2)).$$

$$\alpha_s = 0.019/(1 + \exp((V + 154.51)/11.46)),$$
$$\beta_s = 0.000376/(1 + \exp(-(V + 60.92)/15.79)).$$

I381T mutant was described by the following rate constants:

$$\alpha_m = 0.751/(1 + \exp(-(V + 37.66)/13.71)),$$
$$\beta_m = 5.68/(1 + \exp((V + 129.11)/13.94));$$

$$\alpha_h = 0.082/(1 + \exp((V + 102.39)/17.4)),$$
$$\beta_h = 0.24/(1 + \exp(-(V - 21.4)/17.2)).$$

$$\alpha_s = 0.019/(1 + \exp((V + 154.51)/11.46)),$$
$$\beta_s = 0.000376/(1 + \exp(-(V + 60.92)/15.79)).$$

Sodium current was described by $I_{Na} = g_{max} \times m \times h \times S \times (V_m - E_{Na})$, where g_{max} is maximal conductance, V_m is membrane voltage, $E_{Na} = 65$ mV is sodium reversal potential (Herzog *et al.*, 2001). Steady-state fast- and slow-inactivation, steady-state activation, time constants for activation and deactivation for both wild-type and I381T mutant channels were from our voltage-clamp recordings; fast-inactivation and repriming time constants of wild-type channels were from Vanoye *et al.* (2013); slow-inactivation time constant was from Herzog *et al.* (2001); g_{max} was set to 30 nS (Rush and Waxman, 2004) and our voltage-clamp recordings, which show ~2 nA of current. We assumed a voltage-dependent shift of I381T channel inactivation and repriming kinetics to be equivalent to the $V_{1/2}$ shift of I381T channel steady-state inactivation; slow-inactivation time constant was from Herzog *et al.* (2001). All parameters were adjusted for the respective junction potentials.

In dynamic-clamp recordings we fixed slow-inactivation at −60 mV RMP ($S = 0.027$ resulting in CED dynamic-clamp $g1_{max} = S \times g_{max} = 0.8$ nS, referred to thereafter as 100% $Na_v1.9$ conductance) because we limited stimulation to 2 s trains at 5 Hz where the development of slow-inactivation is not appreciable. Currents evoked by voltage-clamp and action potential-clamp protocols were calculated in 10 µs precision using custom program written in Origin8.5 LabTalk.

Results

DNA analysis

Two mutations in *SCN11A*, the gene encoding $Na_v1.9$, substituting highly conserved residues in membrane-spanning segments, were selected for detailed functional analysis from eight *SCN11A* mutations. Of 459 patients referred to the Maastricht University Medical Centre for possible painful peripheral neuropathy between September 2009 and October 2013, the diagnosis of predominantly small fibre neuropathy was confirmed in 393 patients (Table 1). In 369 of these 393 patients, the diagnosis of definite small fibre neuropathy was made, and this was considered to be pure small fibre neuropathy based on clinical symptoms, abnormal quantitative sensory testing and/or abnormal skin biopsy, in combination with normal nerve conduction studies, in accordance with published criteria (Lauria *et al.*, 2012). In an additional 24 of these

Table 1 Patient characteristics and additional investigations in a cohort of 393 patients diagnosed with painful peripheral neuropathy

Age	Mean 49 years (range 1–80, SD 14.1)
Family history	Positive *n* = 60, negative *n* = 262, unknown *n* = 71
Abnormal intraepidermal nerve fibre density	*n* = 135
Abnormal quantitative sensory testing	*n* = 363
Abnormal nerve conduction studies	*n* = 24

SD = standard deviation.

393 patients, a diagnosis of small fibre neuropathy was made, but on the basis of clinical signs of large fibre involvement or abnormal nerve conduction studies the diagnosis of predominantly small fibre neuropathy together with large fibre dysfunction was made. Thus our overall cohort of 393 patients with a definite diagnosis of painful peripheral neuropathy consisted of 369 patients with pure small fibre neuropathy and 24 patients with small fibre neuropathy together with large fibre dysfunction. In this paper we describe four patients with painful peripheral neuropathy: two patients with pure small fibre neuropathy and two patients with predominantly small fibre neuropathy together with large fibre involvement. From this cohort of 393 patients, *SCN9A* mutations were found in 34 patients (Faber *et al.*, 2012*a*), and *SCN10A* mutations were found in 15 patients (Faber *et al.*, 2012*b*). *SCN11A* was sequenced in those patients without mutations in *SCN9A* and *SCN10A* (Fig. 1A). Additionally, in one patient the variant found in *SCN9A* did not confer hyperexcitability in DRG neurons when assessed by electrophysiology; thus *SCN10A* and *SCN11A* were subsequently tested, which identified a variant in *SCN11A*. Twelve of 345 patients tested, carried eight variants in *SCN11A*: exon 9, c.1142T>C (p.Ile381Thr) ($n = 2$); exon 9, c.1257G>T (p.Lys419Asn) ($n = 2$); exon 12, c.1744G>A (p.Ala582Thr) ($n = 2$); exon 14, c.2042C>A (p.Ala681Asp); exon 15, c.2524G>C (p.Ala842Pro); exon 20, c.3473T>C (p.Leu1158Pro) ($n = 2$); intron 24, c.4057-1G>A; exon 26, c.5067C>G (p.Phe1689Leu). All of the subjects carrying these variants were heterozygous for these new mutations. Of the seven missense variants found in *SCN11A*, four (c.1142T>C, p.Ile381Thr; c.1744G>A (p.Ala582Thr); c.2042C>A (p.Ala681Asp); c.3473T>C, p. Leu1158Pro), in exons 9, 12, 14, and 20, respectively, substituted amino acids in membrane-spanning segments of the channel; the I381T mutation located in domain I transmembrane 6 (DI/S6), and the L1158P mutation located in DIII/S4, were chosen for functional analysis (Fig. 1B).

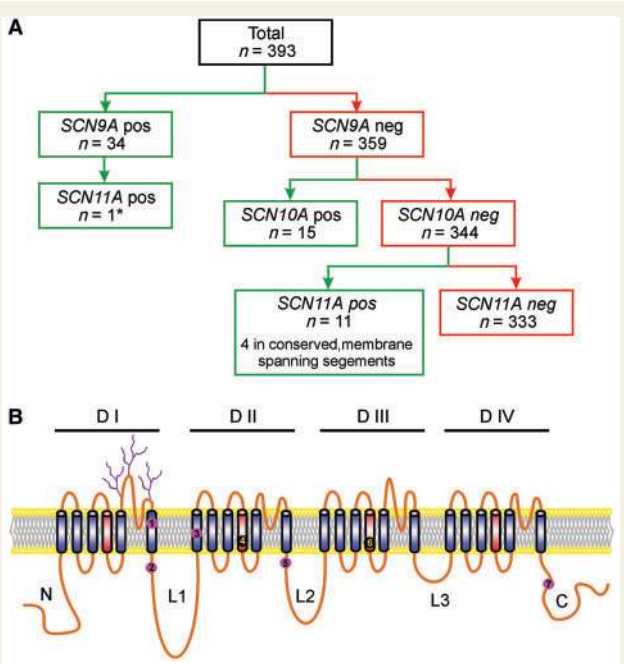

Figure 1 Scheme for patient selection and localization of $Na_v1.9$ variants. (**A**) Scheme for selecting patients with small fibre neuropathy for *SCN11A* screening. **SCN9A* variant c.3799C>G (p.Leu1267Val) did not show abnormalities in cell electrophysiology; therefore, *SCN10A* and *SCN11A* were tested. (**B**) Schematic of sodium channel polypeptide showing the locations of the missense mutations in $Na_v1.9$ in individuals with painful peripheral neuropathy and no mutations in $Na_v1.7$ or $Na_v1.8$. The mutations are: (1) I381T; (2) K419N; (3) A582T; (4) A681D; (5) A842P; (6) L1158P; and (7) F1689L. The mutations I381T and L1158P, which were profiled in this study, were each present in two patients. One additional mutation was found at the 3′ acceptor splice site in intron 24.

The I381T and L1158P mutations were not found in 224 and 470 chromosomes from control populations in The Netherlands and the UK, respectively. The I381T variant was not reported in the dbSNP, EVS and 1000 Genome databases; the L1158P was reported with a low minor allele frequency in the EVS ($n = 8/13006$) and the 1000 Genome ($n = 1/2184$) databases, but was not reported in the dbSNP database ($n = 0/4552$). The mutation I381T substitutes a hydrophobic highly conserved isoleucine with a polar threonine in DI/S6, a pore-lining segment. The mutation L1158P substitutes a hydrophobic residue with a long sidechain, leucine with a proline residue, which introduces a turn in the DIII/S4 of domain 3, the voltage-sensor of this domain (Fig. 1B). *In silico* analysis suggested these mutations to be deleterious.

Clinical description

Patient 1: c.3473T>C; p.Leu1158Pro

A 73-year-old male was referred to our neurology outpatient clinic with a 2-year history of numbness and tingling in both legs, which started after intestinal surgery for colorectal carcinoma, with the symptoms gradually disseminating to his hands. He was not treated with chemotherapy. He also developed cramps and stabbing pain in his feet, and contact with sheets was irritating, and sometimes his hands discoloured white, accompanied with sharp pain. The complaints were not associated with temperature changes or activity. Family history was unremarkable. The patient also complained of hyperhidrosis, dry eyes and mouth, orthostatic dizziness, palpitations and occasionally hot flushes. Pregabalin initially gave some pain relief, but only for a few months.

Physical examination showed no abnormalities, and nerve conduction studies were unremarkable. Quantitative sensory testing showed abnormal thresholds for warmth sensation in both feet and for cold sensation in the right foot. Skin biopsy demonstrated an intraepidermal nerve fibre density of 3.1 per mm, which was normal compared with gender- and age-matched normative values (5th percentile: 2.1 per mm). The patient was diagnosed with small fibre neuropathy. DNA analysis showed no mutations in the *SCN9A* and *SCN10A* genes, however, a new variant was found in the *SCN11A* gene: c.3473T>C; p.Leu1158Pro.

Patient 2: c.3473T > C; p.Leu1158Pro

A 61-year-old female presented with a 2-year history of numbness, tingling and a dull burning pain in the toes and foot soles. She also complained of restless legs and occasional calf cramps, with standing and walking aggravating the complaints. The toes intermittently showed a blue-purple discolouration. The patient also complained of hyperhidrosis, diarrhoea, a dry mouth, dry eyes, palpitations and hot flushes. A low dose of gabapentin (300 mg/day) resulted in pain relief. Medical history showed primary biliary cirrhosis, well-treated hyperthyroidism and a laryngeal carcinoma, treated 10 years before with surgery and radiation therapy. The patient also had a history of herpes zoster attacks of her buttocks. Family history is unremarkable.

Physical examination showed decreased vibration sense at both ankles. Laboratory tests revealed positive anti-mitochondrion antibodies, appropriate to the primary biliary cirrhosis. Blood tests demonstrated elevated liver enzymes, weak bands in the gamma region and vitamin B12 deficiency. Nerve conduction studies were normal. Quantitative sensory testing showed abnormal thresholds for warmth and cold sensation in both feet. A skin biopsy demonstrated an intraepidermal nerve fibre density of 1.0 per mm, which was low compared with gender- and age-matched normative values (5th percentile: 3.2 per mm), which confirmed a diagnosis of small fibre neuropathy. Based on the impaired vibration sense, a diagnosis of predominantly small fibre neuropathy together with large fibre involvement was made. DNA analysis showed no mutations in the *SCN9A* and *SCN10A* genes. A new variant was found in the *SCN11A* gene: c.3473T > C; p.Leu1158Pro.

Patient 3: c.1142T > C; p.Ile381Thr

A 50-year-old male presented with a 10-year history of numbness of the hands, arms and feet, and a family history of joint pain. Low ambient temperatures triggered burning pain in his fingers and toes, sometimes with a red discolouration. In addition, he complained of arthralgia. The pain tended to be more severe in the morning. The patient also complained of hyperhidrosis, diarrhoea, a dry mouth, orthostatic dizziness, palpitations and hot flushes. A combination of nortriptyline, arthrotec and acetaminophen gave some pain relief.

Physical examination showed slightly reduced vibration sense at the toes. Nerve conduction studies demonstrated signs of a moderate peripheral polyneuropathy. Quantitative sensory testing demonstrated abnormal thresholds for warmth sensation in both hands and the left foot. The thresholds for cold sensation were abnormal in the left foot. A skin biopsy demonstrated an intraepidermal nerve fibre density of 4.8 per mm, which was normal (5th percentile: 3.5 per mm; 10th percentile: 4.9 per mm). The patient was diagnosed with predominantly small fibre neuropathy together with large fibre dysfunction. DNA analysis showed no mutations in the *SCN9A* and *SCN10A* genes, however, a variant was found in the *SCN11A* gene: c.1142T > C; p.Ile381Thr.

Patient 4: c.1142T > C; p.Ile381Thr

A 56-year-old female presented with a 5-year history of burning, tingling sensations and a dull, pulsing pain of the fingers and toes. The complaints gradually extended to the upper legs, pubic region, ears and tip of the tongue. Bathing in lukewarm water and a cool breeze diminished the complaints. Contact with sheets and wearing shoes was painful. The patient also complained of hyperhidrosis, diarrhoea, micturation problems, palpitations and hot flushes. Several anti-epileptic drugs caused side effects and were discontinued, and amitriptyline gave no pain relief.

The patient suffered from an autosomal dominant form of Alport's syndrome, located on chromosome 2, characterized by glomerulonephritis, end-stage kidney disease and hearing loss, but at the time of evaluation had normal renal function. Both her mother and sister were also diagnosed with Alport's syndrome. Her mother experienced the same pain complaints as the patient. DNA from the mother was not available for analysis.

Physical examination showed no abnormalities, and nerve conduction studies were normal. Quantitative sensory testing showed abnormal thresholds for warmth sensation in both feet. The thresholds for cold sensation were abnormal in the left foot. A skin biopsy demonstrated an intraepidermal nerve fibre density of 8.1 per mm, which was normal (5th percentile: 4.3 per mm). The patient was diagnosed with small fibre neuropathy. DNA analysis showed a variant (c.3799C > G; p.Leu1267Val) in the *SCN9A* gene. However, this variant did not confer hyperexcitability in DRG neurons when assessed by electrophysiology (unpublished data); thus *SCN10A* and *SCN11A* were subsequently tested, which identified a variant in *SCN11A*:c.1142T > C; p.Ile381Thr.

Functional assessment of L1158P: patch-clamp

Wild-type human $Na_v1.9$ and mutant channels L1158P were each transiently expressed in DRG neurons from $Na_v1.9$ knock-out mice. $Na_v1.9$ currents were obtained by subtracting $Na_v1.8$ sodium currents from the total TTX-resistant sodium currents. To record the total TTX-resistant sodium currents, cells were held at −100 mV with 500 nM TTX in the bath and stepped to membrane potentials from −100 to −20 mV for 100 ms in 5 mV increments. Subsequently, the holding potential was depolarized to −60 mV to inactivate $Na_v1.9$ channels (Cummins *et al.*, 1999), and $Na_v1.8$ currents were elicited by the same protocol as recording the total TTX-resistant currents following a prepulse of 100 ms at −100 mV. The $Na_v1.9$ current was obtained by subtracting the $Na_v1.8$ current from the total TTX-resistant current. Representative voltage-dependent inward currents of wild-type and L1158P displaying the ultra-slow inactivation characteristic of $Na_v1.9$ are presented in Fig. 2A and B, respectively. Although the nominal $Na_v1.9$ channel current density of L1158P mutant channel (97 ± 18 pA/pF; $n = 13$) was smaller than that of wild-type channel (135 ± 36 pA/pF; $n = 16$), the difference did not reach statistical significance ($P > 0.05$). Figure 2C shows the voltage-dependence of activation for wild-type and L1158P channels. The midpoint of activation for L1158P (estimated by fitting with a Boltzmann function) was significantly shifted by −6.7 mV (wild-type: −49.6 ± 2.0 mV, $n = 12$; L1158P: −56.3 ± 1.1 mV, $n = 10$; $P < 0.05$). However, the slope factor was not significantly different between wild-type and L1158P channels (wild-type:

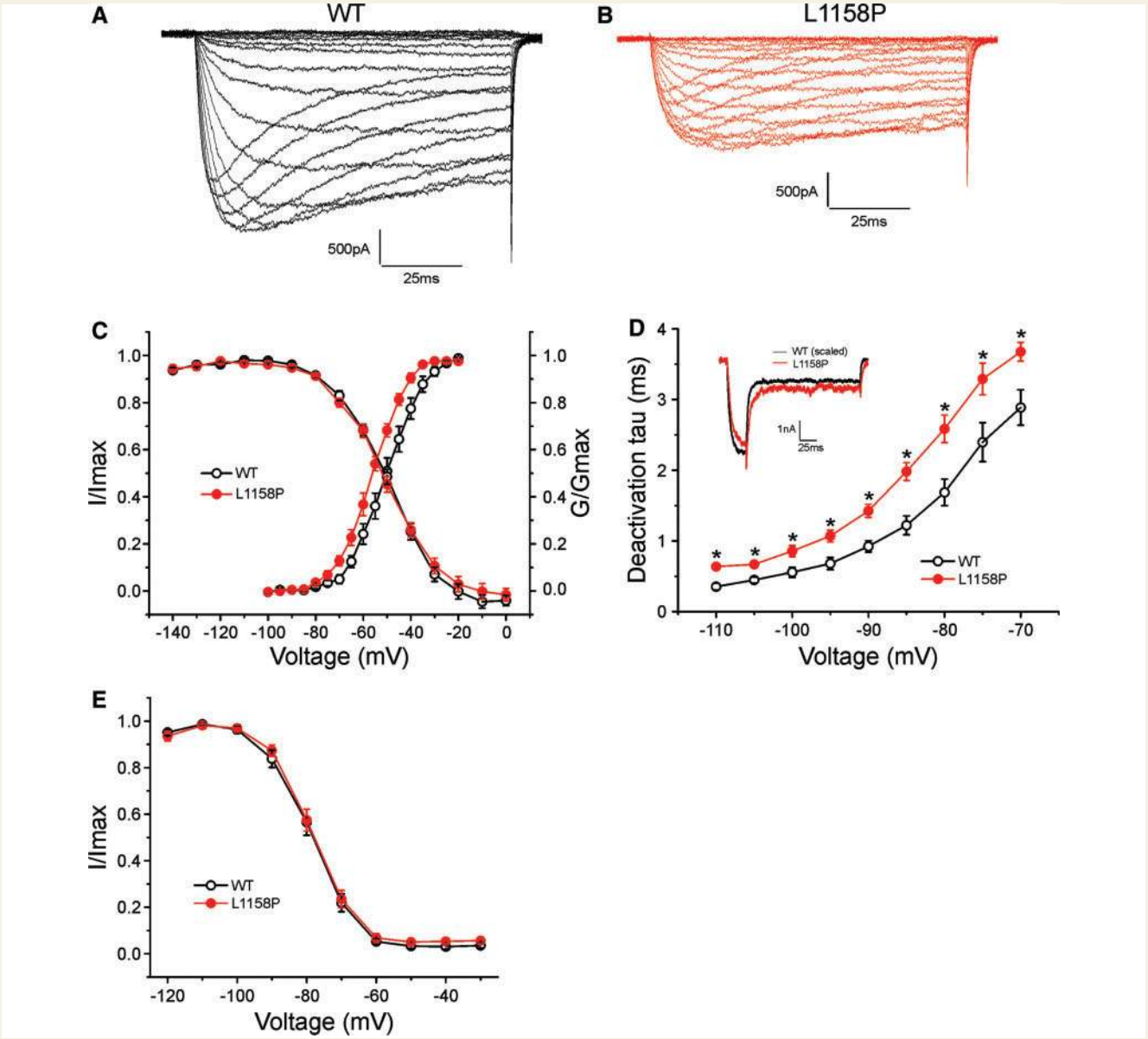

Figure 2 Voltage-clamp analysis of L1158P mutant channels. (**A** and **B**) Representative current traces recorded from DRG neurons expressing wild-type (**A**) or L1158P (**B**) mutant channels. (**C**) Comparison of activation for wild-type (WT) and L1158P mutant channels. L1158P shifts activation by −6.7 mV (wild-type: −49.6 ± 2.0 mV, $n = 12$; L1158P: −56.3 ± 1.1 mV, $n = 10$; $P < 0.05$). Comparison of steady-state fast-inactivation for wild-type and L1158P mutant channels. L1158P does not affect steady-state fast-inactivation (wild-type: −50.5 ± 1.3 mV, $n = 10$; L1158P: −48.8 ± 1.1 mV, $n = 10$; $P > 0.05$). (**D**) Comparison of deactivation time constants. L1158P ($n = 15$) deactivates significantly slower than wild-type ($n = 12$), $^*P < 0.05$. *Inset*: Representative currents recorded from two different neurons expressing wild-type (black) or L1158P (red) sodium channels at a repolarization voltage of −70 mV. The wild-type current peak was scaled to match the L1158P current peak for comparing the kinetics of current decay. (**E**) Steady-state slow-inactivation curves for wild-type and L1158P. Steady-state slow-inactivation was not altered by the L1158P mutation (wild-type: −79.0 ± 1.7 mV, $n = 12$; L1158P: −78.0 ± 1.3 mV, $n = 10$; $P > 0.05$).

7.3 ± 0.5, $n = 12$; L1158P: 7.2 ± 0.5, $n = 10$; $P > 0.05$). Steady-state fast-inactivation was measured using a series of 500 ms prepulses from −140 to 0 mV followed by 50 ms test pulse to −45 mV. As shown in Fig. 2C, the midpoint of fast-inactivation for L1158P mutant channels (−48.8 ± 1.1 mV, $n = 10$) was not significantly different from that of wild-type channels (−50.5 ± 1.3 mV, $n = 10$; $P > 0.05$). The slope factor of fast-inactivation was not significantly different between wild-type and L1158P channels (wild-type: 10.7 ± 0.8, $n = 10$; L1158P: 11.1 ± 0.8, $n = 10$; $P > 0.05$).

The kinetics of deactivation, which reflect the transition from the open to the closed state, were measured using single exponential fits to estimate the time of current decay at potentials from −110 to −70 mV after briefly activating the channels at −45 mV for 25 ms. As shown in Fig. 2D, the rates of current decay of L1158P mutant channels were significantly slower than those of

wild-type channels across all deactivation potentials tested. The inset in Fig. 2D shows the slowed deactivation for L1158P at −70 mV.

We also measured steady-state slow-inactivation, a process that inactivates the channel much more slowly than fast-inactivation, with 30 s prepulses, followed by 100 ms pulses to −100 mV to allow recovery from fast-inactivation, and then a 50 ms test pulse to −45 mV to determine the fraction of $Na_v1.9$ channel current available. As shown in Fig. 2E, the L1158P mutation has no significant effect on steady-state slow-inactivation. The mid-point was −79.0 ± 1.7 mV for wild-type ($n = 12$) and −78.0 ± 1.3 mV for L1158P mutant channels ($n = 10$; $P > 0.05$), respectively. The slope factor of L1158P channels (5.3 ± 0.1, $n = 10$) was not significantly different from that of wild-type channels (5.4 ± 0.3, $n = 12$; $P > 0.05$).

To assess the effect of the L1158P mutation on excitability, we expressed wild-type and L1158P mutant channels in rat small DRG neurons and performed current-clamp recordings (Fig. 3). The input resistance was similar between DRG neurons expressing wild-type channels (702 ± 81 MΩ, $n = 26$) and those expressing L1158P mutant channels (712 ± 95 MΩ, $n = 22$; $P > 0.05$). However, the RMP of DRG neurons that expressed L1158P mutant channels (−50.9 ± 1.0 mV, $n = 22$) was significantly depolarized by 3.5 mV, compared with DRG neurons expressing wild-type channels (−54.4 ± 1.2 mV, $n = 26$; $P < 0.05$) (Fig. 3C).

Current threshold was significantly reduced after expression of L1158P (165 ± 22 pA, $n = 22$), compared with wild-type channels (250 ± 21 pA, $n = 26$; $P < 0.01$) (Fig. 3D). However, there was no significant difference between these two groups of DRG neurons for either voltage threshold (the voltage at which the take-off occurs) (wild-type: −16.8 ± 1.1 mV; L1158P: −16.4 ± 0.9 mV, $P > 0.05$), action potential width at 0 mV (wild-type: 3.30 ± 0.30 ms; L1158P: 3.27 ± 0.25 ms, $P > 0.05$) or action potential amplitude (wild-type: 106.8 ± 1.3 mV; L1158P: 104.9 ± 2.2 mV, $P > 0.05$) between neurons expressing wild-type ($n = 26$) or L1158P ($n = 22$) channels.

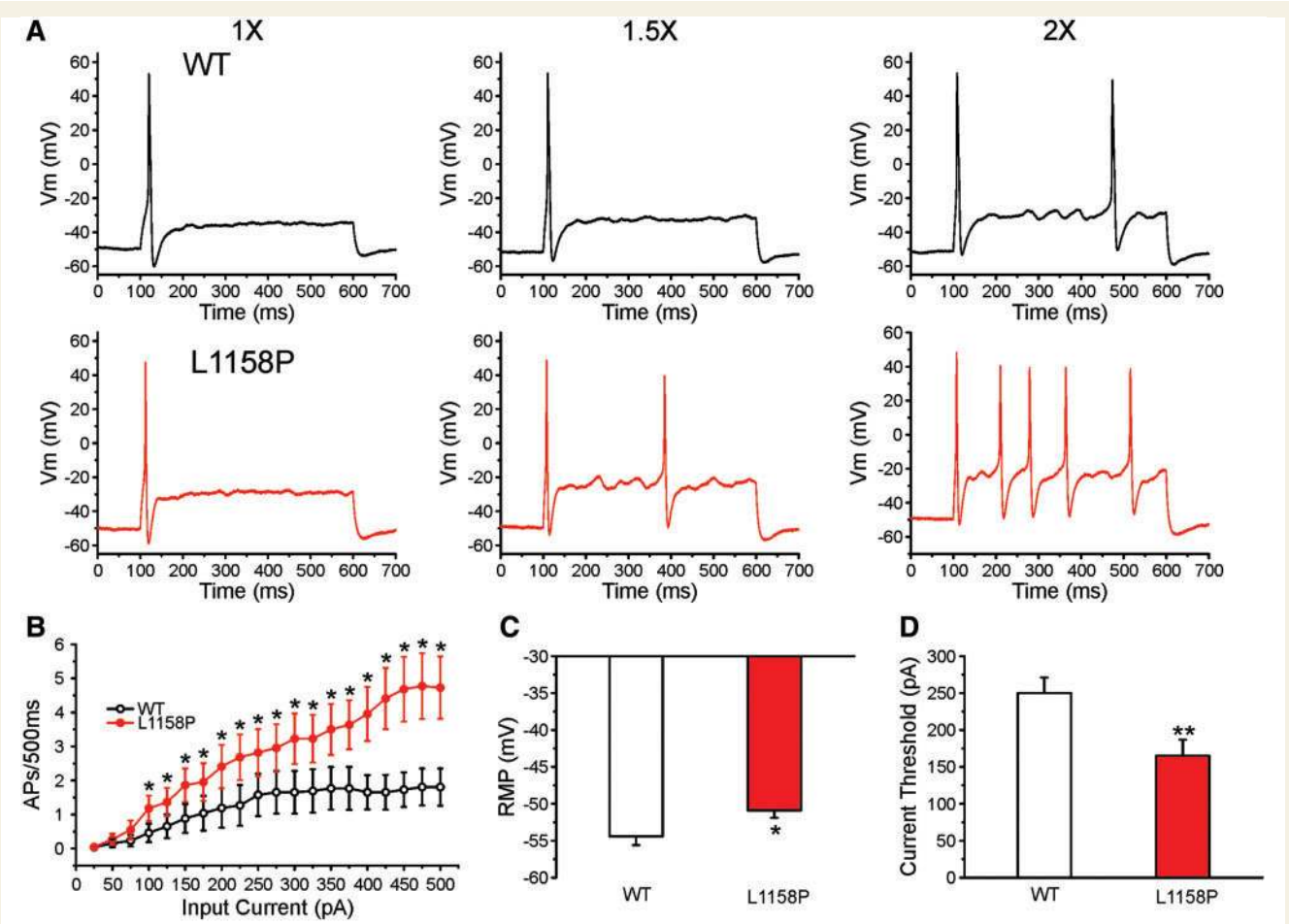

Figure 3 Current-clamp analysis of L1158P mutation. (**A**) Responses of representative DRG neurons expressing wild-type (*upper*) and L1158P (*lower*) channels, respectively, to 500 ms depolarization current steps which are 1×, 1.5× and 2× (*left*, *centre* and *right* traces, respectively) the current threshold for action potential generation. (**B**) Comparison of repetitive action potential firing spike number between DRG neurons expressing wild-type ($n = 26$) and L1158P ($n = 22$) across a range of 500 ms step current injections from 25 to 500 pA; $^*P < 0.05$. (**C**) L1158P significantly depolarized resting membrane potential by 3.5 mV compared with wild-type channels (wild-type: −54.4 ± 1.2 mV, $n = 26$; L1158P: −50.9 ± 1.0 mV, $n = 22$; $^*P < 0.05$). (**D**) Current threshold was reduced significantly after expression of L1158P (165 ± 22 pA, $n = 22$), compared with wild-type (250 ± 21 pA, $n = 26$; $^{**}P < 0.01$). AP = action potential.

To evaluate repetitive action potential firing, we assessed the response of DRG neurons to a series of 500 ms current injections from 25 to 500 pA in 25 pA increments. Figure 3A shows the responses of a representative DRG neuron which expressed wild-type or L1158P mutant channels, to 500 ms current steps at 1×, 1.5× and 2× current threshold. The DRG neuron expressing wild-type channels generated a single spike in response to the current injections at both 1× and 1.5× current threshold, and two spikes to the injection of 2× current threshold. In contrast, the neuron expressing L1158P mutant channels fired two or more action potentials in response to the stimuli of 1.5× current threshold, and five action potentials in response to stimulation at 2× current threshold. Figure 3B shows data for the population of transfected DRG neurons, and clearly demonstrates that neurons expressing the L1158P channels fired significantly more action potentials compared to neurons expressing wild-type channels. Additionally, we found that for both groups of DRG neurons, a small proportion of neurons fired spontaneously; however, we did not detect a significant difference for the portion of spontaneously firing neurons between the two groups (wild-type: 5 of 31 cells, 16%; L1158P: 7 of 29 cells, 24%; $P > 0.05$, *z*-test).

Functional assessment of I381T: patch-clamp

Representative voltage-dependent inward currents of wild-type and I381T, which again display the ultra-slow inactivation characteristic of $Na_v1.9$, are presented in Fig. 4A and B, respectively. The average peak inward current amplitude was not significantly different between wild-type $Na_v1.9$ and I381T (wild-type, -2.39 ± 0.45 nA, $n = 13$; I381T, -3.10 ± 0.81 nA, $n = 14$; $P > 0.05$). When normalized for capacitance, similarly, the average peak current density of I381T (-198 ± 47 pA/pF, $n = 14$) did not differ from that of wild-type (-231 ± 50 pA/pF, $n = 13$; $P > 0.05$).

The voltage-dependence of activation and steady-state fast-inactivation for wild-type and I381T are illustrated in Fig. 4C. Compared with wild-type, the midpoint of activation ($V_{1/2,act}$) was shifted 6.9 mV more negative for I381T (wild-type, -55.3 ± 1.8 mV, $n = 12$; I381T, -62.2 ± 1.4 mV, $n = 10$; $P < 0.01$). The slope factor of I381T, however, remained unaffected (wild-type, 7.93 ± 0.61; I381T, 8.49 ± 0.53, $P > 0.05$). Steady-state fast-inactivation also exhibited a robust change in voltage-dependence. The midpoint voltage ($V_{1/2,fast}$) of I381T was depolarized by 13.3 mV compared to that of wild-type (wild-type, -53.3 ± 1.7 mV, $n = 11$; I381T, -40.0 ± 1.6 mV, $n = 14$; $P < 0.001$). In contrast, the slope factor of I381T was not significantly different from that of wild-type (wild-type, 10.6 ± 1.6; I381T, 12.1 ± 1.0; $P > 0.05$). The combinatorial effect of a hyperpolarizing shift of activation and depolarizing shift of steady-state fast-inactivation markedly increases the predicted window current for I381T mutant channel, compared with wild-type channels.

The deactivation properties of I381T are displayed in Fig. 4D. The I381T mutation ($n = 8$) produced a significant decrease in the rate of current decay across all deactivation potentials tested, compared to wild-type ($n = 12$). For example, the deactivation time constant at −70 mV was 4.84 ± 0.14 ms ($n = 8$) for I381T, increasing by 23% compared to that for wild-type (3.93 ± 0.26 ms, $n = 12$, $P < 0.05$). Representative current traces at a repolarizing potential of −70 mV are presented in the inset of Fig. 4D to illustrate slowed deactivation in I381T transfected DRG neuron.

As a final assessment of the effects of the I381T mutation on voltage-gated sodium currents mediated by $Na_v1.9$, slow-inactivation of the channels was examined using a 50 ms depolarizing pulse at −45 mV after a series of 30 s prepulses from −130 to −30 mV, which are followed by 100 ms pulses to −100 mV to remove fast-inactivation. The peak current at the testing potential of −45 mV was normalized and plotted against the prepulse membrane potential. Slow-inactivation for wild-type and I381T channels are superimposed in Fig. 4E. Fit with a Boltzmann function, the midpoint voltage of slow-inactivation of wild-type was -81.9 ± 4.1 mV ($n = 5$), with a slope factor of 6.98 ± 0.92 ($n = 5$). The I381T mutant channel had a midpoint of slow-inactivation of -82.4 ± 2.1 mV ($n = 6$, $P > 0.05$), and a slope factor of 7.88 ± 1.1 ($n = 6$, $P > 0.05$), neither of which differ significantly from that of wild-type channels.

To assess the effects of I381T on DRG neuronal excitability, we performed current-clamp studies in two groups of rat small DRG neurons transfected with wild-type or I381T channels. There were no significant differences in input resistance (wild-type, 588 ± 54 MΩ; I381T, 673 ± 77 MΩ, $P > 0.05$), action potential amplitude (wild-type, 97.5 ± 3.3 mV; I381T, 102 ± 3.8 mV, $P > 0.05$), action potential width at 0 mV (wild-type, 3.99 ± 0.23 ms; I381T, 3.90 ± 0.33 ms, $P > 0.05$) or voltage threshold at which an all-or-none action potential takes off (wild-type, -18.5 ± 2.0 mV; I381T, -19.6 ± 1.7 mV, $P > 0.05$) between neurons expressing wild-type ($n = 26$) or I381T ($n = 22$) channels. The RMP of neurons expressing I381T, however, was depolarized by 5.5 mV (wild-type, -50.6 ± 1.6 mV; I381T, -45.1 ± 1.4 mV, $P < 0.05$) (Fig. 5C). Current threshold, at which an all-or-none action potential is elicited, was assessed by injecting a series of currents in increments of 5 pA over 200 ms to neurons expressing either wild-type or I381T channels. There is a nearly 50% reduction of current threshold for single action potentials in neurons expressing I381T (wild-type, 236 ± 30 pA; I381T, 138 ± 23 pA, $P < 0.05$) (Fig. 5D).

Representative action potentials triggered by current injections 1×, 1.5× and 2× of current threshold in neurons transfected with either wild-type or I381T channels are illustrated in Fig. 5A. The average numbers of action potentials in wild-type and I381T elicited by graded current injections in 25 pA increments are plotted in Fig. 5B. DRG neurons transfected with I381T fire at a significantly higher frequency than DRG neurons transfected with wild-type in response to similar stimuli from 225 pA to 500 pA.

Expression of the I381T channels also led to an increase in the proportion of spontaneously firing DRG neurons. A representative recording showing sustained spontaneous firing from a DRG neuron expressing I381T mutant channels is shown in Fig. 5E. Only 10% (3 of 29 cells) of DRG neurons expressing wild-type channels fired spontaneously. Expression of I381T, in contrast, resulted in >5-fold increase in the proportion of spontaneously firing cells (52%, 24 of 46 cells), significantly more than for wild-type ($P < 0.001$, *z*-test).

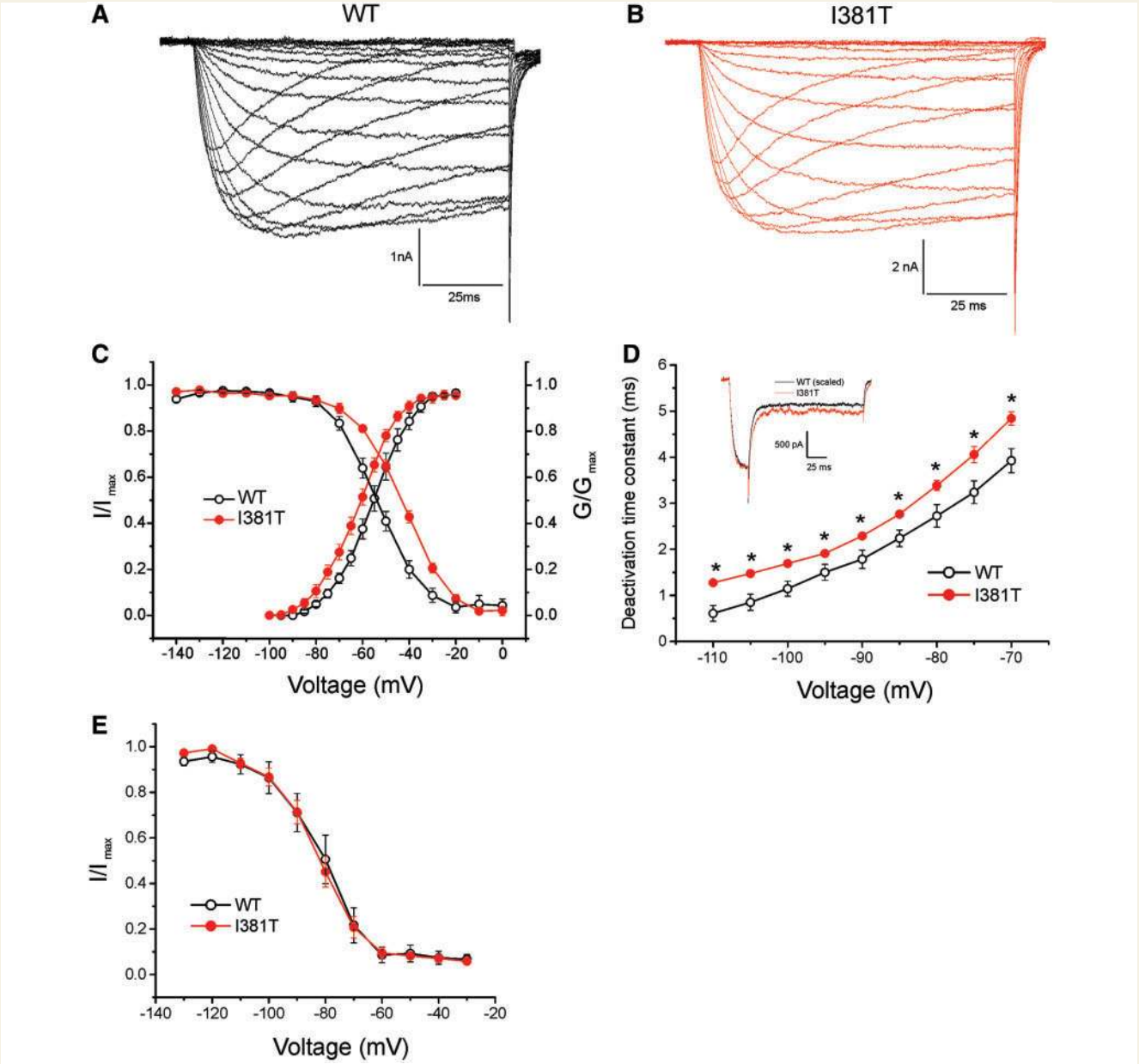

Figure 4 Voltage-clamp analysis of I381T mutant channels. Inward currents recorded from a small-diameter DRG neuron expressing wild-type $Na_v1.9$ (**A**) or I381T mutant (**B**) sodium channels. (**C**) Comparison of the voltage dependence of activation (wild-type, -55.3 ± 1.8 mV, $n = 12$; I381T, -62.2 ± 1.4 mV, $n = 10$; $P < 0.01$) and steady-state fast-inactivation (wild-type, -53.3 ± 1.7 mV, $n = 11$; I381T, -40.0 ± 1.6 mV, $n = 14$; $P < 0.001$) for wild-type and I381T channels. (**D**) Voltage-dependence of deactivation time constants for wild-type ($n = 12$) and I381T ($n = 8$) channels. *Inset*: Representative currents recorded from two different neurons expressing wild-type (black) or I381T (red) sodium channels at a repolarization voltage of -70 mV. The wild-type current peak was scaled to match the I381T current peak for comparing the kinetics of current decay. (**E**) Voltage-dependence of steady-state slow-inactivation for wild-type (-81.9 ± 4.1 mV, $n = 5$) and I381T channels (-82.4 ± 2.1 mV, $n = 6$, $P > 0.05$).

Depolarization of resting membrane potential and dorsal root ganglion neuron excitability

The L1158P and I381T mutations depolarized RMP of DRG neurons by 3.5 mV and 5.5 mV, respectively. Although most current-clamp studies show that depolarized RMP due to $Na_v1.7$ mutations result in DRG neuron hyperexcitability (Rush *et al.*, 2006; Faber *et al.*, 2012*a*; Han *et al.*, 2012*b*), Leipold *et al.* (2013) have suggested that depolarization can reduce the excitability of DRG neurons. To examine the hypothesis that the depolarization of RMP contributes to the decrease in current threshold for single action potential generation, we measured changes in current thresholds when injected currents were used to hold DRG neurons at membrane potentials

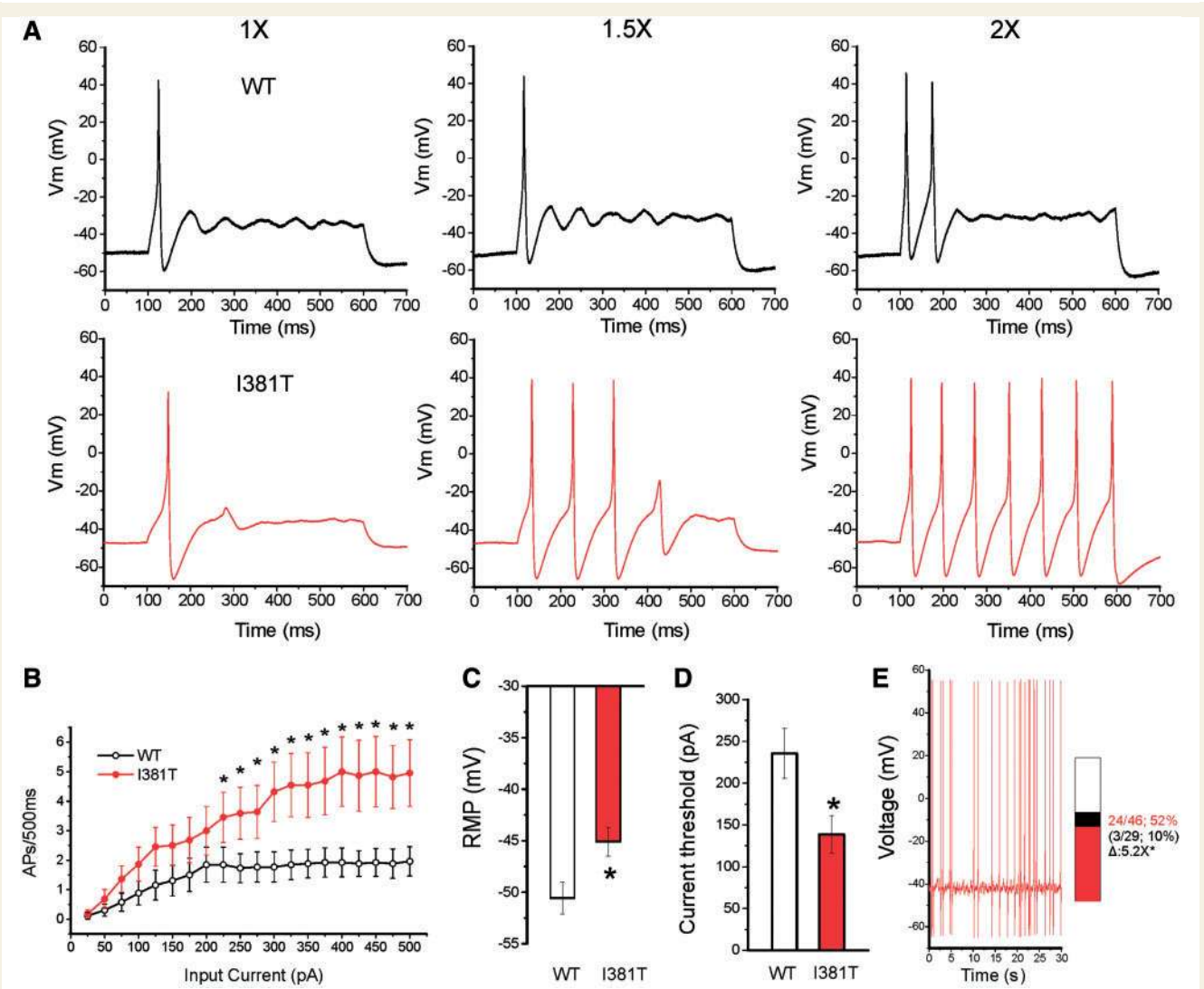

Figure 5 Current-clamp analysis of I381T mutation. (**A**) Responses of a neuron expressing wild-type or I381T channels to 500 ms depolarizing current steps that are 1×, 1.5× and 2× of the current threshold. (**B**) Summary of firing frequency data. The total number of action potentials (APs) elicited by the indicated depolarizing current steps from 25 to 500 pA in 25 pA increments was compared between two groups of neurons expressing wild-type ($n = 26$) or I381T ($n = 22$) channels. (**C**) RMP of neurons expressing I381T (-45.1 ± 1.4 mV) was depolarized by 5.5 mV as compared to that of wild-type channels (-50.6 ± 1.6 mV, $P < 0.05$). (**D**) Current threshold was significantly reduced after expressing I381T channels (wild-type, 236 ± 30 pA; I381T, 138 ± 23 pA; $P < 0.05$). (**E**) Representative recording of spontaneous firing in a DRG neuron expressing I381T mutant channels. Trace was recorded for 30 s without current injection. *Inset*: Bar graph showing the proportion of spontaneous firing cells for DRG neurons expressing I381T (red) is >5-fold compared to that of wild-type (black); numbers to the right of the bar graph show values for wild-type (10%, lower value in parentheses) and I381T (52%, upper value). *$P < 0.001$ *z*-test.

5 mV more depolarized than their RMP, similar to the shift produced by the I381T channel. The RMP for adult rat DRG neurons was -58.6 ± 1.1 mV ($n = 14$). We found that depolarization of RMP by 5 mV decreased current threshold from 252 ± 46 pA to 189 ± 39 pA ($n = 14$, $P < 0.001$, paired *t*-test). We also performed the converse experiment and found that hyperpolarization of RMP by 5 mV increased current threshold to 319 ± 72 pA ($n = 14$, $P < 0.01$, paired *t*-test). In all cells tested, there is a decrease in current threshold when RMP is depolarized by 5 mV and an increase in current thresholds when RMP is hyperpolarized by 5 mV. On average, a 5 mV depolarization of RMP led to a significant reduction in current threshold of action potential in DRG neurons by $27.2 \pm 3.9\%$ while a 5 mV hyperpolarization of RMP resulted in an increase in current threshold by $26.5 \pm 3.5\%$ (Fig. 6).

Assessment of physiological levels of I381T by dynamic clamp recordings

Our current-clamp observations indicate that transfection of DRG neurons with mutant $Na_v1.9$ channels renders them hyperexcitable, compared to similar neurons transfected with wild-type $Na_v1.9$ channels. However, transfection of DRG neurons by

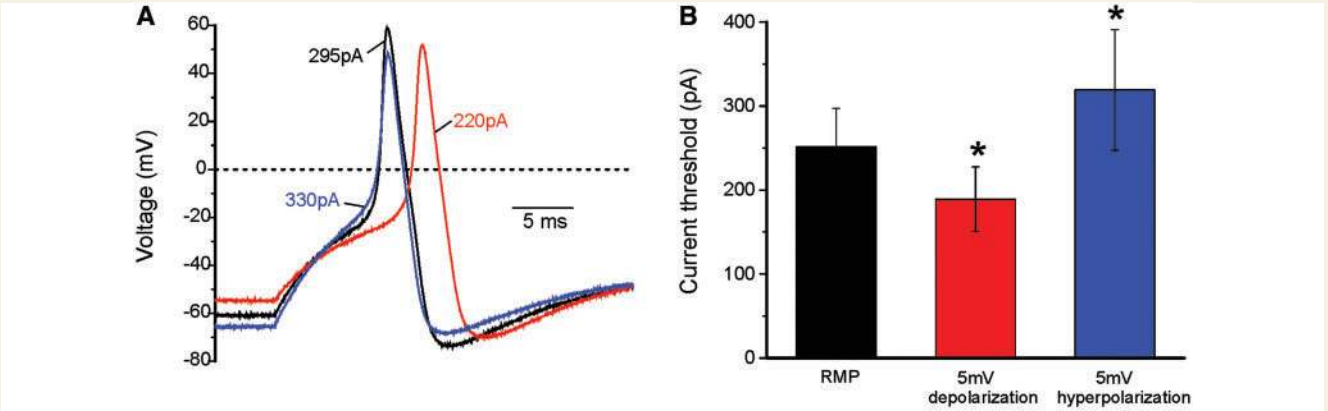

Figure 6 Depolarization of RMP of DRG neurons by 5 mV reduces current threshold for action potential. (**A**) Representative action potentials recorded from a native adult rat DRG neuron at its RMP (black), at membrane potential depolarized by current injection 5 mV (red) or hyperpolarized by 5 mV (blue). Arrows and numbers indicate current thresholds at different membrane potentials. (**B**) The current threshold was reduced when the neurons were held at membrane potentials 5 mV depolarized compared to RMP and increased when they were held at membrane potentials 5 mV hyperpolarized compared to RMP. *$P < 0.001$, paired *t*-test.

wild-type or mutant channels does not permit precise control of the level of expression of the transfected channels and, by definition, produces supra-physiological levels of the channel. Given the contention by Leipold *et al*. (2013) that gain-of-function mutations of $Na_v1.9$ can impair action potential generation in DRG neurons, we decided to use dynamic clamp (Sharp *et al.*, 1993; Kemenes *et al.*, 2011; Samu *et al.*, 2012) to study the effects of expressing wild-type and mutant $Na_v1.9$ at physiological levels. Although currently available dynamic clamp software only permits inclusion of two kinetic particles (and thus is not strictly comparable to current-clamp), it provides the opportunity to assess the effect of the expression of precisely calibrated, physiologically relevant levels of wild-type and mutant $Na_v1.9$ channels on DRG neuron excitability.

In the present study we used dynamic clamp recordings to introduce physiologically relevant, calibrated levels of wild-type and I381T conductances into small DRG neurons. As human subjects carrying the I381T mutation are heterozygous, we started with $Na_v1.9$-null DRG neurons and added back 100% wild-type or 50%/50% mixture of wild-type and I381T current (WT:IT). First we performed *in silico* evaluation of wild-type and I381T mutant channels. Figure 7A shows computer simulation of current traces obtained from wild-type (blue) and I381T (orange) $Na_v1.9$ channel model $I_{Na} = g_{max} \times m \times h \times s \times (V_m - E_{Na})$ which we used for these experiments. Figure 7C shows the $Na_v1.9$ kinetic model steady-state fast-inactivation (solid), steady-state activation (solid) and steady-state slow-inactivation (dashed) (left panel); activation time constant (middle panel) and inactivation time constant (right panel). The wild-type model is shown in blue and I381T is shown in orange. Computed currents were evoked in response to voltage steps ranging from −90 mV to 60 mV (in 10 mV increments) applied from a −110 mV holding potential. The model cell was equipotential 15 pF sphere with 0.0018 S/cm^2 current density. We used spontaneous firing from a small DRG neuron (Fig. 7B, top) as a voltage command to study modelled wild-type (blue) and I381T (orange) $Na_v1.9$ currents associated with the action potential shown (Fig. 7B, bottom).

As shown in Fig. 7D, dynamic-clamp recordings of action potentials evoked by current pulses of threshold intensity in control DRG neurons from $Na_v1.9$ knockout mice with no added $Na_v1.9$ (black), and after dynamic-clamp addition of 100% wild-type conductance (blue) and (50% wild-type + 50% I381T) conductance (red) demonstrate that wild-type $Na_v1.9$ reduces current threshold, with I831T mutant channels reducing threshold even further. Figure 7E shows action potential repetitive firing evoked by a 5 Hz train of current pulses in control (top, black) and after dynamic-clamp addition of 100% wild-type (middle, blue) and (50% wild-type + 50% I381T) conductance (bottom, red), and illustrates increased firing frequency due to expression of the mutant channel.

Finally, we found by dynamic clamp (Fig. 7F) that addition of wild-type $Na_v1.9$ depolarizes DRG RMP by 9.4 mV ± 0.7 mV (wild-type), and that substitution of I381T for 50% of wild-type $Na_v1.9$ depolarizes RMP by12.7 mV ± 0.7 mV. Thus, we found, in a series of 13 $Na_v1.9$-null DRG neurons in which we first measured control RMP (no $Na_v1.9$), then added 100% wild-type $Na_v1.9$, or substituted a 50%/50% mixture of wild-type $Na_v1.9$ and I381T, and finally returned to control conditions (no $Na_v1.9$) and again measured RMP: −61.7 mV ± 0.7 mV (control); −52.3 mV ± 0.8 mV (wild-type); −49.1 mV ± 0.7 mV (WT:IT); −62.1 mV ± 0.8 mV (control). Wild-type versus WT:IT ($P < 0.01$, *t*-test, $n = 13$). Similarly, we found that expression of wild-type $Na_v1.9$ reduces current threshold by −37.8% ± 3.3% (wild-type); with 50% substitution by I381T producing a reduction of −48.7% ± 3.5% (WT:IT) ($P < 0.05$, *t*-test, $n = 13$) [current threshold: 116.9 pA ± 9.70 pA (control); 71.5 pA ± 5.6 pA (wild-type); 59.2 pA ± 5.3 pA (WT:IT); 116.2 pA ± 10.0 pA (control). Wild-type versus WT:IT ($P > 0.05$, *t*-test, $n = 13$)]. The number of action potentials evoked by a 10-pulses stimulus was increased from 4.2 ± 0.6 (wild-type), to 6.6 ± 0.7 (WT:IT) ($P < 0.05$, Mann-Whitney, $n = 11$).

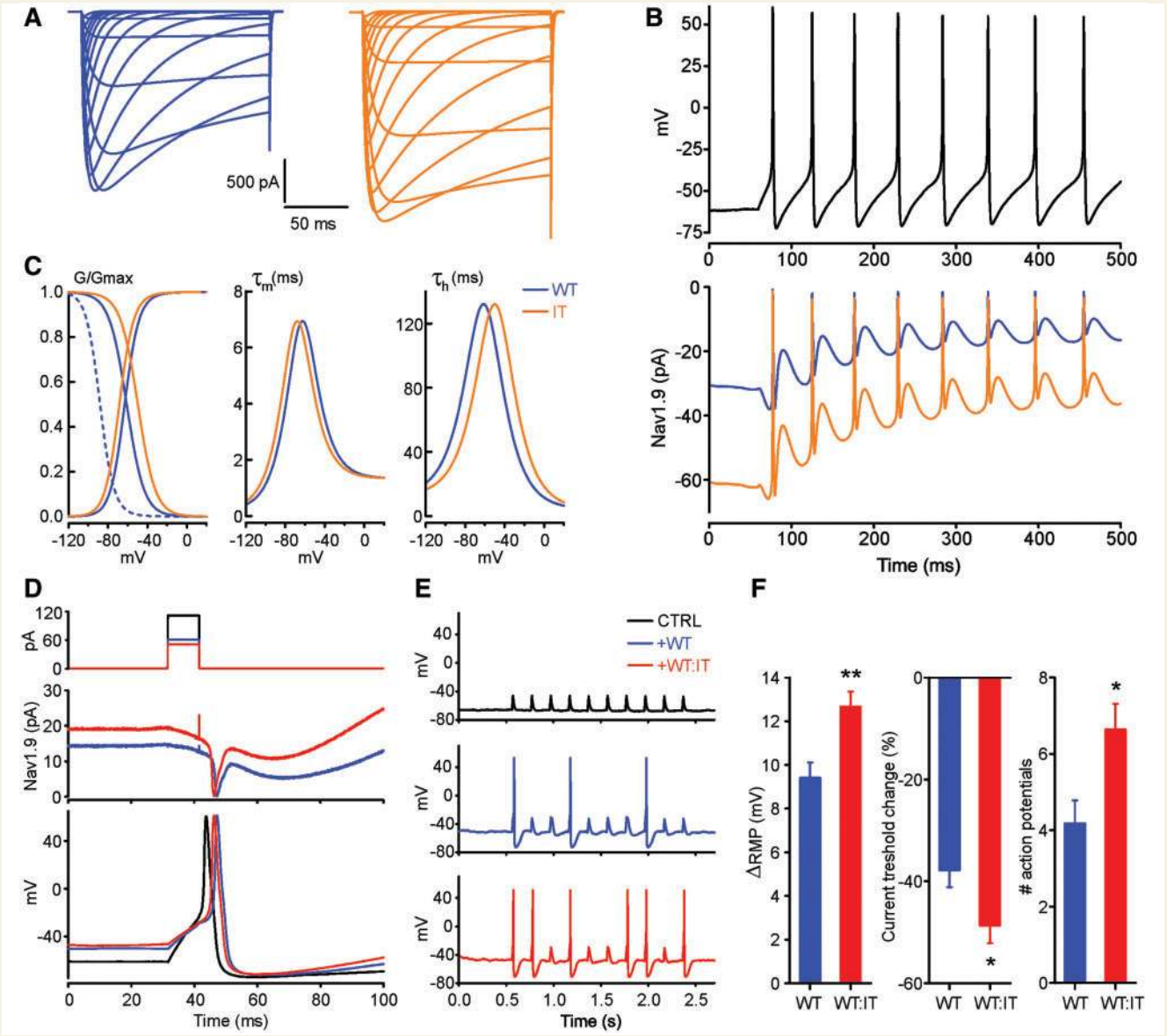

Figure 7 Dynamic clamp recording of DRG neuron firing using physiological levels of wild-type or mutant $Na_v1.9$ currents. (**A**) Current traces obtained from wild-type (blue) and I381T (orange) $Na_v1.9$ channel model $I_{Na} = g_{max} \times m \times h \times s \times (V_m - E_{Na})$. Currents were evoked by voltage steps ranged from −90 mV to 60 mV (in 10 mV increment) applied from −110 mV holding potential. The model cell was equipotential 15 pF sphere with 0.0018 S/cm^2 current density. (**B**, *top*) Repetitive firing of a spontaneously active small DRG neuron. (**B**, *bottom*) Modelled wild-type (blue) and I381T (orange) $Na_v1.9$ currents obtained in response to the voltage command shaped in the form of the action potential shown in **B** (*top*). (**C**) $Na_v1.9$ kinetic model steady-state fast inactivation (solid), steady-state activation (solid) and steady-state slow inactivation (dashed) are presented on the *left* panel; activation time constant and inactivation time constant are shown on the *middle* and *right* panel, respectively. Wild-type model is shown in blue and I381T is shown in orange. (**D**) Dynamic-clamp recordings of action potentials evoked by current pulses of threshold intensity in control (black), after dynamic-clamp addition of 100% wild-type conductance (blue) and (50% wild-type + 50% I381T) conductance (red). Stimulation current pulses are shown on top panel, dynamic-clamp currents are shown on the middle panel and action potentials are presented on the bottom panel. (**E**) Action potential repetitive firing evoked by a 5 Hz train of current pulses in control (*top*, black) and after dynamic-clamp addition of 100% wild-type (*middle*, blue) and (50% wild-type + 50% I381T) conductance (*bottom*, red). (**F**) ΔRMP: 9.4 mV ± 0.7 mV (wild-type); 12.7 mV ± 0.7 mV (WT:IT) ($P < 0.01$, *t*-test, $n = 13$). RMP: −61.7 mV ± 0.7 mV (control); −52.3 mV ± 0.8 (wild-type); −49.1 mV ± 0.7 mV (WT:IT); −62.1 mV ± 0.8 mV (control). Wild-type versus WT:IT ($P < 0.01$, *t*-test, $n = 13$). Current threshold change: −37.8% ± 3.3% (wild-type); −48.7% ± 3.5% (WT:IT) ($P < 0.05$, *t*-test, $n = 13$). Current threshold: 116.9 pA ± 9.70 pA (control); 71.5 pA ± 5.6 pA (wild-type); 59.2 pA ± 5.3 pA (WT:IT); 116.2 pA ± 10.0 pA (control). Wild-type versus WT:IT ($P > 0.05$, *t*-test, $n = 13$). Number of action potentials: 4.2 ± 0.6 (wild-type); 6.6 ± 0.7 (WT:IT) ($P < 0.05$, Mann-Whitney, $n = 11$).

Discussion

Our results identified eight mutations of *SCN11A*, the gene encoding sodium channel $Na_v1.9$, in 12 individuals from a cohort of 345 individuals with painful peripheral neuropathy, who did not carry mutations of *SCN9A* or *SCN10A*. Four of these mutations substituted highly conserved amino acids in membrane-spanning segments of the channel, while three were located within cytoplasmic loops and the C-terminus, and one affected the 3′ splice acceptor site of intron 24. We assessed two of these mutations by voltage- and current-clamp, and studied one of these using dynamic-clamp, and found that they confer gain-of-function attributes on $Na_v1.9$ and are proexcitatory in DRG neurons. Similar to $Na_v1.7$ and $Na_v1.8$, $Na_v1.9$ is expressed by DRG neurons with a preferential distribution in small-diameter, non-peptidergic neurons (Dib-Hajj *et al.*, 1998, 2002), most of which are nociceptors (Fang *et al.*, 2002), and has been found within free nerve terminals in the skin and cornea (Black and Waxman, 2002; Dib-Hajj *et al.*, 2002; Persson *et al.*, 2010), as well as nodose ganglion neurons (Schild and Kunze, 1997; Matsumoto *et al.*, 2007) including aortic baroreceptors (Qiao *et al.*, 2009) and visceral afferent neurons that innervate the intestine (Rugiero *et al.*, 2003; Padilla *et al.*, 2007) and, under some conditions, the urinary bladder (Black *et al.*, 2003). Thus gain-of-function mutations in this channel might be expected to contribute to pain, autonomic dysfunction and axonal degeneration in patients with peripheral neuropathy.

In addition to prominent complaints of numbness, tingling and pain in the distal extremities, the patients noted a number of complaints usually associated with autonomic dysfunction, including a sensation of dry eyes, diarrhoea, urinary problems, palpitations, and orthostatic dizziness. Consistent with these clinical complaints, $Na_v1.9$ channels are present within free nerve terminals in the cornea (Black and Waxman, 2002) and it has been proposed that hyperactivity of corneal nociceptors can trigger a sensation of ocular dryness (Belmonte and Gallar, 2011; Rosenthal and Borsook, 2012). $Na_v1.9$ is also present within nodose ganglion neurons (Schild and Kunze, 1997; Matsumoto *et al.*, 2007) including aortic baroreceptors (Qiao *et al.*, 2009) and visceral afferent neurons innervating the intestine (Rugiero *et al.*, 2003; Padilla *et al.*, 2007) and, in some injury models, the urinary bladder (Black *et al.*, 2003). Although the effects of mutant $Na_v1.9$ channels in these cell-types has not be studied, it is possible that altered patterns of activity in these neurons contribute to the autonomic complaints in the patients we describe

Although families were not available for study, and thus pathogenicity cannot be inferred from segregation of phenotype with carriers of these alleles, each of the two functionally-profiled mutations was identified in two independent patients. The rare occurrence in control populations and genomic databases and the gain-of-function attributes demonstrated by our functional characterization strongly suggest that these mutations are pathogenic. The two substitutions produced pro-excitatory changes in the gating properties of the mutant $Na_v1.9$ channels as revealed by voltage-clamp recordings in DRG neurons where this channel is normally expressed. By current-clamp, we found that both mutations reduce current threshold and increase firing frequency in response to suprathreshold stimuli, which would be expected to lower threshold for, or increase intensity of, evoked pain. We also observed that the I381T mutation induced spontaneous firing of small DRG neurons, which include nociceptors, and would be expected to contribute to spontaneous pain.

Previous studies of DRG neuron excitability via current-clamp recording has been conducted following the expression of mutant sodium channels, compared to the excitability of neurons expressing the corresponding wild-type channel (for a recent review, see Dib-Hajj *et al.*, 2013). However, these studies cannot control for the level of expression of the recombinant channel, which is generally added to the full complement of the endogenous sodium currents in the transfected neurons. In an effort to study the effect of a mutant $Na_v1.9$ channel on the excitability of DRG neurons using physiological levels of the mutant current in relation to the endogenous $Na_v1.9$ current we used dynamic clamp (Sharp *et al.*, 1993; Kemenes *et al.*, 2011; Samu *et al.*, 2012). Using this approach, we showed that substituting 50% of wild-type $Na_v1.9$ current by the corresponding I381T current (a manoeuvre that mimics the presence of one mutant allele) causes a significant depolarization of the RMP neurons and induces hyperexcitability of DRG neurons, providing additional support for the contention that the nociceptors of an individual heterozygous for this mutation can become hyperexcitable, consistent with the pain phenotype.

Our findings are consistent with those of a recent study that linked gain-of-function mutations in $Na_v1.9$ to familial episodic pain (Zhang *et al.*, 2013). Zhang *et al*. (2013) reported that the mutations R225C and A808G, which segregated with pain phenotype in individuals from two multi-generation families, cause an increase in the current density of $Na_v1.9$ without affecting the channel's gating properties, and increased excitability of DRG neurons expressing the mutant channel without affecting RMP of these neurons. Together with the current results, this study establishes a link between $Na_v1.9$ mutations, which increase current density or confer gain-of-function attributes onto gating properties of the $Na_v1.9$ channel and painful disorders, including the rare disease familial episodic pain as shown by Zhang *et al*. (2013), and the more common disorder painful peripheral neuropathy as shown here.

In contrast with our observations on painful neuropathies, and those of Zhang *et al*. (2013) in familial episodic pain, another study reported that a gain-of-function mutation of $Na_v1.9$ causes a form of congenital insensitivity to pain (Leipold *et al.*, 2013). Leipold *et al*. (2013) reported that the *de novo* mutation L811P in $Na_v1.9$, identified in two unrelated individuals with this form of congenital insensitivity to pain using whole exome sequencing, causes a -28 mV shift in voltage-dependence of activation, leading to a depolarization of $\sim$6.7 mV of RMP of DRG neurons; they argued that this depolarization causes resting inactivation of most voltage-gated sodium channels in these neurons and thus leads to hypoexcitability, consistent with the phenotype of pain insensitivity. However, as shown here and in many studies (Rush *et al.*, 2006; Faber *et al.*, 2012*a*, *b*; Han *et al.*, 2012*b*), depolarization of RMP of DRG neurons causes hyperexcitability of these neurons. Additionally, specifically mimicking a 5 mV

depolarization in RMP produced by the $Na_v1.7$ A863P erythromelalgia mutation or the $Na_v1.9$ I381T by direct current injection into DRG neurons, instead of that produced by the transfection of mutant channels, leads to hyperexcitability of DRG neurons (Harty and Waxman, 2007) (Fig. 6). Thus, the hypoexcitability of mouse DRG neurons that express the $Na_v1.9$ L811P mutation cannot be explained by the shift in RMP of these neurons.

Hyperexcitability of small DRG neurons, most of which are nociceptors, upon depolarization of their RMP in the range of 5–6 mV is due to the presence in these cells of $Na_v1.8$, a channel that is unique by possessing activation and steady-state inactivation with voltage-dependencies that are depolarized by 20–40 mV with respect to other voltage-gated sodium channels (Catterall *et al.*, 2005). Indeed, depolarization of the RMP of neurons that do not produce $Na_v1.8$, for example sympathetic neurons of superior cervical ganglion, causes hypoexcitability of these neurons (Rush *et al.*, 2006; Han *et al.*, 2012*b*), which can be reversed by expressing $Na_v1.8$ in these neurons (Rush *et al.*, 2006). The pain insensitivity phenotype reported by Leipold *et al*. (2013) might have been explained by a lack of $Na_v1.8$ in the DRG neurons that they studied, but this seems unlikely since $Na_v1.8$ is expressed in >90% of small DRG neurons in the mouse (Shields *et al.*, 2012). An alternative possibility is that extreme hyperexcitability of $Na_v1.9$-expressing DRG neurons, due to the −28 mV shift in voltage-dependence of activation produced by the $Na_v1.9$ L811P mutation, leads to sustained subnormality or fatigue of this group of cells, while leaving the population of hypoexcitable DRG neurons that do not express $Na_v1.8$ intact, but Leipold *et al*. (2013) did not present any evidence for this type of functional abnormality.

Our results confirm the observation that gain-of-function mutations of $Na_v1.9$ can produce painful syndromes (Zhang *et al.*, 2013) and extend the link between gain-of-function mutations in $Na_v1.9$ and pain from rare genetic model diseases to a more common disorder, painful peripheral neuropathy. Together with our earlier studies linking gain-of-function mutations of $Na_v1.7$ (Estacion *et al.*, 2011; Faber *et al.*, 2012*a*; Han *et al*., 2014; Han *et al.*, 2012*a*, *b*; Hoeijmakers *et al.*, 2012*b*) and $Na_v1.8$ (Faber *et al.*, 2012*b*; Huang *et al.*, 2013) and peripheral neuropathy, the present results suggest the potential for treatment of pain associated with peripheral neuropathy via the targeting of peripheral sodium channels.

Acknowledgements

We thank Lawrence Macala, Peng Zhao, Shujun Liu, Fadia Dib-Hajj, Palak Shah, Ilse Driesmans, Aline Kosten, Linda Meekels and Diane Merckx for their technical assistance in this project.

Funding

This work was supported in part by grants from the Rehabilitation Research Service and Medical Research Service, Department of Veterans Affairs (SGW and SDH), and grant #602273 from the European Union Seventh Framework Programme FP7/2007-2013. The Center for Neuroscience & Regeneration Research is a Collaboration of the Paralyzed Veterans of America with Yale University.

References

Ahn HS, Vasylyev DV, Estacion M, Macala LJ, Shah P, Faber CG, et al. Differential effect of D623N variant and wild-type Na1.7 sodium channels on resting potential and interspike membrane potential of dorsal root ganglion neurons. Brain Res 2013; 1529: 165–77.

Atkins JF, Wills NM, Loughran G, Wu CY, Parsawar K, Ryan MD, et al. A case for "StopGo": reprogramming translation to augment codon meaning of GGN by promoting unconventional termination (Stop) after addition of glycine and then allowing continued translation (Go). RNA 2007; 13: 803–10.

Baker MD, Chandra SY, Ding Y, Waxman SG, Wood JN. GTP-induced tetrodotoxin-resistant Na + current regulates excitability in mouse and rat small diameter sensory neurones. J Physiol 2003; 548 (Pt 2): 373–82.

Belmonte C, Gallar J. Cold thermoreceptors, unexpected players in tear production and ocular dryness sensations. Invest Ophthalmol Vis Sci 2011; 52: 3888–92.

Black JA, Cummins TR, Yoshimura N, de Groat WC, Waxman SG. Tetrodotoxin-resistant sodium channels Na(v)1.8/SNS and Na(v)1.9/NaN in afferent neurons innervating urinary bladder in control and spinal cord injured rats. Brain Res 2003; 963: 132–8.

Black JA, Frezel N, Dib-Hajj SD, Waxman SG. Expression of Nav1.7 in DRG neurons extends from peripheral terminals in the skin to central preterminal branches and terminals in the dorsal horn. Mol Pain 2012; 8: 82.

Black JA, Waxman SG. Molecular identities of two tetrodotoxin-resistant sodium channels in corneal axons. Exp Eye Res 2002; 75: 193–9.

Catterall WA, Goldin AL, Waxman SG. International Union of Pharmacology. XLVII. Nomenclature and structure-function relationships of voltage-gated sodium channels. Pharmacol Rev 2005; 57: 397–409.

Cummins TR, Dib-Hajj SD, Black JA, Akopian AN, Wood JN, Waxman SG. A novel persistent tetrodotoxin-resistant sodium current in SNS-null and wild-type small primary sensory neurons. J Neurosci 1999; 19: RC43.

Dib-Hajj S, Black JA, Cummins TR, Waxman SG. NaN/Nav1.9: a sodium channel with unique properties. Trends Neurosci 2002; 25: 253–9.

Dib-Hajj SD, Choi JS, Macala LJ, Tyrrell L, Black JA, Cummins TR, et al. Transfection of rat or mouse neurons by biolistics or electroporation. Nat Protoc 2009; 4: 1118–26.

Dib-Hajj SD, Cummins TR, Black JA, Waxman SG. Sodium channels in normal and pathological pain. Annu Rev Neurosci 2010; 33: 325–47.

Dib-Hajj SD, Tyrrell L, Black JA, Waxman SG. NaN, a novel voltage-gated Na channel, is expressed preferentially in peripheral sensory neurons and down-regulated after axotomy. Proc Natl Acad Sci USA 1998; 95: 8963–8.

Dib-Hajj SD, Tyrrell L, Cummins TR, Black JA, Wood PM, Waxman SG. Two tetrodotoxin-resistant sodium channels in human dorsal root ganglion neurons. FEBS Lett 1999; 462: 117–20.

Dib-Hajj SD, Yang Y, Black JA, Waxman SG. The $Na_V1.7$ sodium channel: from molecule to man. Nat Rev Neurosci 2013; 14: 49–62.

Estacion M, Han C, Choi JS, Hoeijmakers JG, Lauria G, Drenth JP, et al. Intra- and interfamily phenotypic diversity in pain syndromes associated with a gain-of-function variant of NaV1.7. Mol Pain 2011; 7: 92.

Faber CG, Hoeijmakers JG, Ahn HS, Cheng X, Han C, Choi JS, et al. Gain of function $Na_V1.7$ mutations in idiopathic small fiber neuropathy. Ann Neurol 2012a; 71: 26–39.

Faber CG, Lauria G, Merkies IS, Cheng X, Han C, Ahn HS, et al. Gain-of-function Nav1.8 mutations in painful neuropathy. Proc Natl Acad Sci USA 2012b; 109: 19444–9.

Fang X, Djouhri L, Black JA, Dib-Hajj SD, Waxman SG, Lawson SN. The presence and role of the tetrodotoxin-resistant sodium channel $Na_V1.9$ (NaN) in nociceptive primary afferent neurons. J Neurosci 2002; 22: 7425–33.

Han C, Hoeijmakers JG, Ahn HS, Zhao P, Shah P, Lauria G, et al. $Na_V1.7$-related small fiber neuropathy: impaired slow-inactivation and DRG neuron hyperexcitability. Neurology 2012a; 78: 1635–43.

Han C, Hoeijmakers JG, Liu S, Gerrits MM, Te Morsche RH, Lauria G, et al. Functional profiles of SCN9A variants in dorsal root ganglion neurons and superior cervical ganglion neurons correlate with autonomic symptoms in small fibre neuropathy. Brain 2012b; 135 (Pt 9): 2613–28.

Han C, Vasylyev D, Macala LJ, Gerrits MM, Hoeijmakers JG, Bekelaar KJ, et al. The G1662S NaV1.8 mutation in small fibre neuropathy: impaired inactivation underlying DRG neuron hyperexcitability. J Neurol Neurosurg Psychiatry 2014; 85: 499–505.

Harty TP, Waxman SG. Inactivation properties of sodium channel Nav1.8 maintain action potential amplitude in small DRG neurons in the context of depolarization. Mol Pain 2007; 3: 12.

Herzog RI, Cummins TR, Waxman SG. Persistent TTX-resistant Na+ current affects resting potential and response to depolarization in simulated spinal sensory neurons. J Neurophysiol 2001; 86: 1351–64.

Hoeijmakers JG, Faber CG, Lauria G, Merkies IS, Waxman SG. Small-fibre neuropathies–advances in diagnosis, pathophysiology and management. Nat Rev Neurol 2012a; 8: 369–79.

Hoeijmakers JG, Han C, Merkies IS, Macala LJ, Lauria G, Gerrits MM, et al. Small nerve fibres, small hands and small feet: a new syndrome of pain, dysautonomia and acromesomelia in a kindred with a novel NaV1.7 mutation. Brain 2012b; 135 (Pt 2): 345–58.

Huang J, Yang Y, Zhao P, Gerrits MM, Hoeijmakers JG, Bekelaar K, et al. Small-fiber neuropathy Nav1.8 mutation shifts activation to hyperpolarized potentials and increases excitability of dorsal root ganglion neurons. J Neurosci 2013; 33: 14087–97.

Kemenes I, Marra V, Crossley M, Samu D, Staras K, Kemenes G, et al. Dynamic clamp with StdpC software. Nat Protoc 2011; 6: 405–17.

Klugbauer N, Lacinova L, Flockerzi V, Hofmann F. Structure and functional expression of a new member of the tetrodotoxin-sensitive voltage-activated sodium channel family from human neuroendocrine cells. EMBO J 1995; 14: 1084–90.

Lauria G, Merkies IS, Faber CG. Small fibre neuropathy. Curr Opin Neurol 2012; 25: 542–9.

Leipold E, Liebmann L, Korenke GC, Heinrich T, Giesselmann S, Baets J, et al. A de novo gain-of-function mutation in SCN11A causes loss of pain perception. Nat Genet 2013; 45: 1399–404.

Luke GA, de Felipe P, Lukashev A, Kallioinen SE, Bruno EA, Ryan MD. Occurrence, function and evolutionary origins of '2A-like' sequences in virus genomes. J Gen Virol 2008; 89 (Pt 4): 1036–42.

Matsumoto S, Yoshida S, Ikeda M, Tanimoto T, Saiki C, Takeda M, et al. Effect of 8-bromo-cAMP on the tetrodotoxin-resistant sodium (Nav 1.8) current in small-diameter nodose ganglion neurons. Neuropharmacology 2007; 52: 904–24.

Ostman JA, Nassar MA, Wood JN, Baker MD. GTP up-regulated persistent Na+ current and enhanced nociceptor excitability require $Na_V1.9$. J Physiol 2007; 586: 1077–87.

Padilla F, Couble ML, Coste B, Maingret F, Clerc N, Crest M, et al. Expression and localization of the Nav1.9 sodium channel in enteric neurons and in trigeminal sensory endings: implication for intestinal reflex function and orofacial pain. Mol Cell Neurosci 2007; 35: 138–52.

Persson AK, Black JA, Gasser A, Fischer T, Waxman SG. Sodium-calcium exchanger and multiple sodium channel isoforms in intra-epidermal nerve terminals. Mol Pain 2010; 6: 84.

Qiao GF, Li BY, Zhou YH, Lu YJ, Schild JH. Characterization of persistent TTX-R Na+ currents in physiological concentration of sodium in rat visceral afferents. Int J Biol Sci 2009; 5: 293–7.

Rosenthal P, Borsook D. The corneal pain system. Part I: the missing piece of the dry eye puzzle. Ocul Surf 2012; 10: 2–14.

Rugiero F, Mistry M, Sage D, Black JA, Waxman SG, Crest M, et al. Selective expression of a persistent tetrodotoxin-resistant Na+ current and NaV1.9 subunit in myenteric sensory neurons. J Neurosci 2003; 23: 2715–25.

Rush AM, Dib-Hajj SD, Liu S, Cummins TR, Black JA, Waxman SG. A single sodium channel mutation produces hyper- or hypoexcitability in different types of neurons. Proc Natl Acad Sci USA 2006; 103: 8245–50.

Rush AM, Waxman SG. PGE_2 increases the tetrodotoxin-resistant $Na_v1.9$ sodium current in mouse DRG neurons via G-proteins. Brain Res 2004; 1023: 264–71.

Ryan MD, Drew J. Foot-and-mouth disease virus 2A oligopeptide mediated cleavage of an artificial polyprotein. EMBO J 1994; 13: 928–33.

Samu D, Marra V, Kemenes I, Crossley M, Kemenes G, Staras K, et al. Single electrode dynamic clamp with StdpC. J Neurosci Methods 2012; 211: 11–21.

Schild JH, Kunze DL. Experimental and modeling study of Na+ current heterogeneity in rat nodose neurons and its impact on neuronal discharge. J Neurophysiol 1997; 78: 3198–209.

Sharp AA, O'Neil MB, Abbott LF, Marder E. Dynamic clamp: computer-generated conductances in real neurons. J Neurophysiol 1993; 69: 992–5.

Shields SD, Ahn HS, Yang Y, Han C, Seal RP, Wood JN, et al. $Na_V1.8$ expression is not restricted to nociceptors in mouse peripheral nervous system. Pain 2012; 153: 2017–30.

Tate S, Benn S, Hick C, Trezise D, John V, Mannion RJ, et al. Two sodium channels contribute to the TTX-R sodium current in primary sensory neurons. Nat Neurosci 1998; 1: 653–5.

Tesfaye S, Boulton AJ, Dyck PJ, Freeman R, Horowitz M, Kempler P, et al. Diabetic neuropathies: update on definitions, diagnostic criteria, estimation of severity, and treatments. Diabetes Care 2010; 33: 2285–93.

Vanoye CG, Kunic JD, Ehring GR, George AL Jr. Mechanism of sodium channel NaV1.9 potentiation by G-protein signaling. J Gen Physiol 2013; 141: 193–202.

Zhang XY, Wen J, Yang W, Wang C, Gao L, Zheng LH, et al. Gain-of-Function mutations in SCN11A cause familial episodic pain. Am J Hum Genet 2013; 93: 957–66.